Acta Astronautica 166 (2020) 482–492

Contents lists available at ScienceDirect

Acta Astronautica

journal homepage: www.elsevier.com/locate/actaastro

Collocated attitude and vibrations control for square solar sails with tip vanes

Soroosh Hassanpour*, Christopher J. Damaren

University of Toronto Institute for Aerospace Studies, Toronto, Ontario, M3H 5T6, Canada

ARTICLE INFO

Keywords:
Solar sail
Attitude control
Vibrations control
Dynamics
Finite element
Collocated controller
Spillover

ABSTRACT

This paper is devoted to developing collocated attitude and vibrations controllers for a square solar sail spacecraft containing four pre-tensioned triangular sails supported by flexible diagonal booms and four reflective control vanes at boom tips. Since the control torques for attitude control are created by the solar radiation pressure forces on the tip vanes, the attitude control problem is effectively non-collocated. The present work identifies collocated sensing for the tip vane forces which furnishes a passive input-output model. Various controllers are developed which furnish attitude and vibrations control. A finite-element-based linear structural model is used to evaluate the developed controllers and examine the controller-structure interactions.

1. Introduction

Solar sailing is a method of harnessing the momentum carried by sunlight photons, known as solar radiation pressure (SRP), via the use of large sail-like structures to propel a spacecraft in space [1]. Thrust of a solar sail spacecraft is directly affected by its attitude and reflective sails' shapes (deformations). Attitude and vibrations controls are therefore required to steer a solar sail in space and to ensure that it follows the desired mission trajectory [1]. However, conventional attitude control strategies, based on using control moment gyros, reaction wheels, and thrusters, may not be effective for a large solar sail whose mass is distributed over a large area, giving it a relatively large moment of inertia. Large control moments, needed to effectively control the attitude of such a spacecraft, may require large and heavy conventional actuators that negatively impact the efficiency of the solar sail [2,3]. Control moment gyros and reaction wheels are additionally not appropriate since applying large concentrated moments to the ultra-flexible structure of the solar sail may result in some undesired deformations and even failures. Propellant-based attitude control systems (thrusters) are also not suitable considering the long mission lifetime and propellantless intention of solar sails [4,5].

There are non-conventional attitude control strategies, particularly proposed for solar sails, that take into account the unique characteristics of them. A large class of attitude control strategies for solar sails contains those that allow a controlled offset between the solar sail's center of mass and center of pressure to generate required control torques from the SRP. Attitude controllers based on gimballed masses, sliding masses, shifted sails, billowed sails, and sails with variable reflectivity are among the strategies of this class [2–7]. Another class includes strategies that make use of added reflective vanes, with one or two rotational degrees of freedom (DOFs) with respect to the solar sail and located as far as possible from the solar sail's center, to produce required control torques from the SRP thrust on each vane and the vane position with respect to the sail's center [1,5,8–12]. Note that tilted sails method [6] basically works based on the same principles as the tip-vane methods and can be considered as a method of this category.

The strategies of the first class may appear more straightforward to be implemented. However, they have some disadvantages as they usually cannot produce any moment about the axis normal to the sail surface (billowed sails method is claimed to not have this disadvantage [6]) and as they lose their effectiveness when the solar sail rotates away from the sunlight direction (the solar sail is uncontrollable and may become unrecoverable when the axis normal to the sail surface is perpendicular to the sunlight direction). The strategies of the second class, in particular when two-DOF vanes are employed, do not have any of these problems. The two-DOF vanes can rotate towards the sun and generate control forces and moments regardless of the sail orientation with respect to the sunlight direction. The second class strategies suffer from the facts that packaging and deploying the control vanes (along with the main sails) can be challenging and that the control vanes lose their effectiveness when shadowed by the main sails.

There are many studies that have examined the aforementioned attitude control strategies on rigid-body models of solar sails [2–7]. However, in recent years, larger and lighter solar sails have been

* Corresponding author.
E-mail address: soroosh.hassanpour@utoronto.ca (S. Hassanpour).

https://doi.org/10.1016/j.actaastro.2019.07.038
Received 22 October 2018; Received in revised form 9 May 2019; Accepted 14 July 2019
Available online 15 October 2019
0094-5765/

proposed and attracted lots of attention as a key enabling technology for use in new explorations of the solar system [8,13]. These higher performance solar sails cannot be rendered under rigid-body assumptions and require incorporation of the flexibility effects [14,15]. Yet, there are only a few preliminary studies that have considered examining the interactions between the attitude controllers and the structural dynamics of the solar sails [1,11,14–16]. Among these few studies, only Thomas et al. [14] and Jin et al. [16] have tried to account for the solar sail structural dynamics when designing their attitude controllers. Finally, to the best of the authors' knowledge, active vibration suppression/control of solar sails has not been touched upon in the literature.

Using tip vanes, the control torque for attitude control is produced by the force acting on the tip vanes which are non-collocated with attitude and rate measurements on a central hub. In a flexible structure, this typically leads to a non-minimum phase input-output map which can lead to spillover instabilities. This problem can be ameliorated if collocated actuation and sensing is realized. One of our contributions is the identification of collocated sensing corresponding to the tip vane force actuation. An additional benefit is that these measurements furnish active damping of the vibration modes in addition to attitude control.

It should be emphasized that the torques provided by tip vanes scale with the dimension of the sails, the time scales associated with attitude control are long as these are tied to those of the orbital maneuvers, and the time scales associated with vibration are long given the low vibration frequencies. Given these facts, the power required to actuate the vanes is relatively low although the energy required is potentially large over long periods of time.

This paper is devoted to developing attitude and vibrations controllers for a traditional square solar sail with four triangular sails stretched between diagonal booms. The controllers use forces generated by four two-DOF reflective vanes located at the tips of the booms to reorient the solar sail in space and damp out its structural vibrations. The controllers will take into account the structural dynamics of the solar sail to ensure their interactions with the flexible modes of the spacecraft do not lead to any instability problems.

2. Solar sail structural dynamics model

A number of structural dynamic models are available for square solar sails with triangular sails and diagonal support booms. These models are either the over-simplified boom-dominant flexible models where the sails are neglected and only the support booms are taken into account [11,17] or the computationally-expensive geometrically nonlinear finite element models (FEMs) where the in- and out-of-plane deformations of sails and booms are dynamically coupled together [1,13]. Considering their disadvantages [12,18], none of these models are appropriate for the purpose of this study. Instead, a new FEM-based linear structural model, recently developed by the current authors [12,18], will be used within this work to develop and examine attitude and vibrations controllers for solar sails. The suggested linear structural model takes into account the effect of pre-tensioned sail membranes (there is a static coupling between in- and out-of-plane deformations of the sails and booms) and allows powerful modal analysis tools [19–22] to be used for model truncation (order reduction) and model-based optimal controller development.

Consider the square solar sail shown in Fig. 1 which is composed of four triangular sails and four diagonal support booms attached to a central hub [13,23–25]. The triangular sails are stretched between and supported by the diagonal booms. Also, assume that four vanes are attached to the tips of the support booms as attitude and vibrations control actuators [4,5,13,24]. Based on the FEM-based linear structural model, the dynamic equations of such a solar sail can be written as [12]:

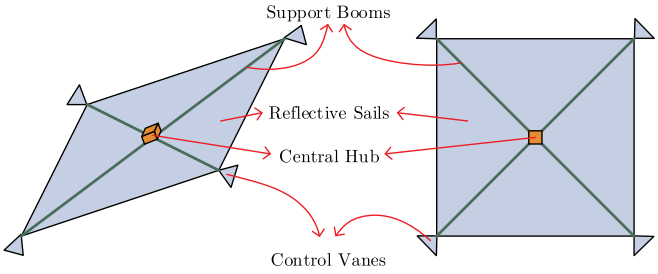

Fig. 1. Schematic configuration of a square solar sail.

$$\mathcal{M}\ddot{\boldsymbol{q}} + \mathcal{K}\boldsymbol{q} = Q, \tag{1}$$

where any passive structural damping is neglected, $\boldsymbol{q} \in \mathbb{R}^n$ is the matrix of generalized coordinates (n will denote the number of generalized coordinates throughout), and $\mathcal{M}$, $\mathcal{K}$, and Q are the finite element mass, stiffness, and generalized force matrices.

Considering small rotational displacements at the central hub of the solar sail, the generalized coordinate matrix and its time derivatives would have the form:

$$\ddot{\boldsymbol{q}} = \begin{bmatrix} \ddot{\boldsymbol{U}} \\ \dot{\boldsymbol{\Omega}} \\ \ddot{\boldsymbol{u}} \end{bmatrix}, \qquad \dot{\boldsymbol{q}} = \begin{bmatrix} \dot{\boldsymbol{U}} \\ \boldsymbol{\Omega} \\ \dot{\boldsymbol{u}} \end{bmatrix}, \qquad \boldsymbol{q} = \begin{bmatrix} \boldsymbol{U} \\ \boldsymbol{\Theta} \\ \boldsymbol{u} \end{bmatrix}, \tag{2}$$

where $\boldsymbol{U} \in \mathbb{R}^3$ is the translational displacement vector of the solar sail hub represented in a body-fixed frame $\mathcal{F}_B$ (attached to the solar sail center as shown in Fig. 2), $\boldsymbol{\Omega} \in \mathbb{R}^3$ is the rotational velocity vector of the solar sail hub represented in $\mathcal{F}_B$, $\boldsymbol{\Theta} \in \mathbb{R}^3$ is the (infinitesimal) rotational displacement vector of the solar sail hub described in $\mathcal{F}_B$, and $\boldsymbol{u}$ is the column matrix of all elastic displacements at nodal points of the FEM. Note that $\boldsymbol{U}$ and $\boldsymbol{\Theta}$ are known as rigid body translational and rotational displacements, respectively.

For solar sails with large rigid-body rotational displacements the integrals of $\ddot{\boldsymbol{U}}$, $\dot{\boldsymbol{U}}$, and $\boldsymbol{\Omega}$ in Eq. (1) would become meaningless (non-physical) quantities. In such cases, the linear dynamic equations in Eq. (1) should be complemented with some (nonlinear) kinematic equations to enable integration of $\ddot{\boldsymbol{U}}$ and $\boldsymbol{\Omega}$ and calculation of the rigid body translational and rotational displacements. Using quaternions (Euler parameters) to parameterize the finite (large) rotations, these differential kinematic equations will be:

$$\begin{aligned} \ddot{\boldsymbol{U}}_I &= (\boldsymbol{1} - 2\varepsilon^T\varepsilon\boldsymbol{1} + 2\varepsilon\varepsilon^T + 2\eta\varepsilon^\times)\ddot{\boldsymbol{U}}, \\ \begin{bmatrix} \dot{\varepsilon} \\ \dot{\eta} \end{bmatrix} &= \frac{1}{2}\begin{bmatrix} -\boldsymbol{\Omega}^\times & \boldsymbol{\Omega} \\ -\boldsymbol{\Omega}^T & \boldsymbol{0} \end{bmatrix}\begin{bmatrix} \varepsilon \\ \eta \end{bmatrix}, \end{aligned} \tag{3}$$

where $\square^T$ represents the transpose operator, $\square^\times$ denotes the skew-symmetric cross product matrix associated with a vector, $\boldsymbol{1}$ is the identity matrix, $\varepsilon \in \mathbb{R}^3$ and η are the vector and scalar parts of the

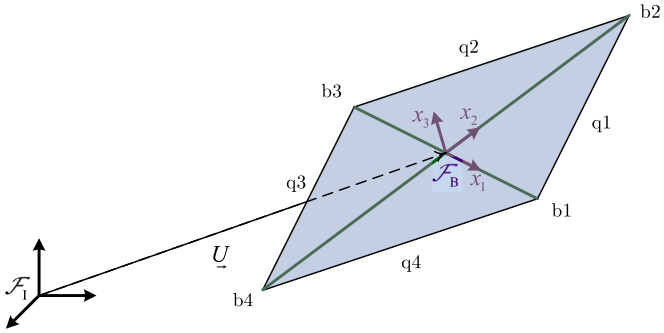

Fig. 2. Square solar sail with four booms and four quadrants along with inertial and body frames.

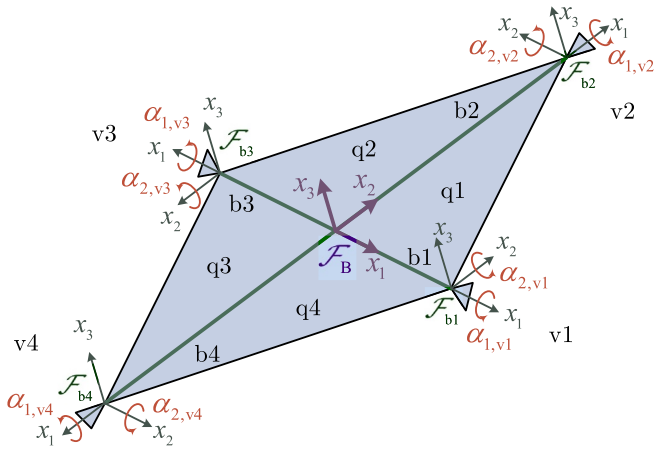

Fig. 3. Solar sail with four two-DOF control tip vanes along with body and vane frames.

quaternion, and ${}^{\mathrm{I}}\ddot{\boldsymbol{U}}$ is the description of translational acceleration vector in $\mathscr{F}_{\mathrm{I}}$. Despite integrals of $\ddot{\boldsymbol{U}}$ that do not have a physical meaning, successive integration of ${}^{\mathrm{I}}\ddot{\boldsymbol{U}}$ results in translational velocities and displacements in $\mathscr{F}_{\mathrm{I}}$, *i.e.* ${}^{\mathrm{I}}\dot{\boldsymbol{U}}$ and ${}^{\mathrm{I}}\boldsymbol{U}$.

Because visualization of encountered rotations from a given quaternion set is not obvious, when presenting the simulation results, the solar sail rigid body rotations will be expressed in terms of x_1 - x_2 - x_3 Euler angles, denoted by θ_1, θ_2, and θ_3 representing sequential rigid-body rotations of solar sail around x_1, x_2, and x_3 axes of the rotating body frame $\mathscr{F}_{\mathrm{B}}$. Moreover, note that the dynamic equations in Eqs. (1) and (3) are valid for solar sails with small rigid body translational accelerations $\ddot{\boldsymbol{U}}$, small rigid body rotational accelerations and velocities $\dot{\boldsymbol{\Omega}}$ and $\boldsymbol{\Omega}$, and small elastic deformations $\ddot{\boldsymbol{u}}$, $\dot{\boldsymbol{u}}$, and $\boldsymbol{u}$.

3. Solar sail with 2-DOF control tip vanes

Now consider the square solar sail shown in Fig. 3 with four double-sided reflective control tip vanes, each having two rotational DOFs with respect to the boom supporting it (defined in more details in Ref. [12]). As shown in Fig. 3, let a boom frame $\mathscr{F}_{\mathrm{b}}$ to be attached to each boom at its tip (where a control vane is connected). Each boom frame $\mathscr{F}_{\mathrm{b}}$ is such that its first axis is parallel to the boom, pointing toward the outside of the solar sail, and its third axis is parallel to the third axis of the body frame $\mathscr{F}_{\mathrm{B}}$. The boom frames rotate with the booms and the solar sail but not with the vanes. The two angular DOFs of each vane are denoted by α_1 and α_2 representing the rotations of the vane about the first and the second axes of the associated boom frame; each vane is first rotated about the second axis of $\mathscr{F}_{\mathrm{b}}$ by α_2, followed by a rotation about the first axis of $\mathscr{F}_{\mathrm{b}}$ by α_1. Since vanes are double-sided reflective, one can assume $-\frac{\pi}{2} \leq \alpha_1, \alpha_2 \leq \frac{\pi}{2}$ [12].

In the control problem, the goal is to first determine the overall required (desired) control forces and moments that should be exerted on the solar sail and then use a control allocation algorithm to solve for the 8 independent control inputs, *i.e.* 8 vane angles, that would result in such overall forces and moments. Considering the highly nonlinear mapping between the resultant forces and moments of the vanes and the rotational DOFs of the vanes, an indirect control allocation approach is taken in this work. In this allocation approach, the forces that each vane must produce are firstly calculated from the overall required forces and moments and then the vane's rotational DOFs are solved for by using an optimization problem [12].

Due to the small size of the vanes relative to the solar sail, the vanes can be assumed to be rigid and flat. Additionally, the dynamics of the vanes can be neglected and the force generated on each vane can be simplified as a concentrated point force vector normal to the vane's surface and exerted at the tip of the boom supporting that vane. Out of three components of each vane's force vector in $\mathscr{F}_{\mathrm{b}}$, only those perpendicular (lateral) to the support boom, *i.e.* ${}^{\mathrm{b}}f_{2,\mathrm{v}}$ and ${}^{\mathrm{b}}f_{3,\mathrm{v}}$, have noteworthy contribution to the dynamics of the solar sail and are of interest for attitude and vibrations control purposes [1,9]. Therefore, in total there are 8 vanes lateral forces (4 vanes multiplies by 2 lateral forces per vane) that can be considered as control inputs.

Having the desired lateral control forces of each vane (as devised by the control allocation algorithm), *i.e.* ${}^{\mathrm{b}}f_{2,\mathrm{v,c}}$ and ${}^{\mathrm{b}}f_{3,\mathrm{v,c}}$, one can use the following two-variable optimization to find α_1 and α_2 of that vane [12]:

$$\begin{aligned} &\underset{\alpha_1,\alpha_2}{\text{minimize}} \quad w_1({}^{\mathrm{b}}f_{2,\mathrm{v,c}} - {}^{\mathrm{b}}f_{2,\mathrm{v}})^2 + w_2({}^{\mathrm{b}}f_{3,\mathrm{v,c}} - {}^{\mathrm{b}}f_{3,\mathrm{v}})^2, \\ &\text{subject to} \quad -\frac{\pi}{2} \leq \alpha_1 \leq \frac{\pi}{2}, \\ &\qquad\qquad -\frac{\pi}{2} \leq \alpha_2 \leq \frac{\pi}{2}, \end{aligned} \tag{4}$$

where w_1 and w_2 are dimensionless weighting coefficients ($0 \leq w_1, w_2 \leq 1$) and note that actual lateral vane forces ${}^{\mathrm{b}}f_{2,\mathrm{v}}$ and ${}^{\mathrm{b}}f_{3,\mathrm{v}}$ are relatively complex functions of α_1 and α_2 and $\boldsymbol{s}$, *i.e.* the sun unit vector expressed in $\mathscr{F}_{\mathrm{B}}$.

Below the force limit of each vane (actuator's saturation point), one can assume that desired and actual lateral control forces are equal. Then, the desired control lateral forces of four tip vanes may be directly combined as a control input vector $\boldsymbol{z}$:

$$\boldsymbol{z} = [{}^{\mathrm{b}}f_{2,\mathrm{v1,c}}\ {}^{\mathrm{b}}f_{3,\mathrm{v1,c}}\ {}^{\mathrm{b}}f_{2,\mathrm{v2,c}}\ {}^{\mathrm{b}}f_{3,\mathrm{v2,c}}\ {}^{\mathrm{b}}f_{2,\mathrm{v3,c}}\ {}^{\mathrm{b}}f_{3,\mathrm{v3,c}}\ {}^{\mathrm{b}}f_{2,\mathrm{v4,c}}\ {}^{\mathrm{b}}f_{3,\mathrm{v4,c}}]^T, \tag{5}$$

that can be used to rewrite the dynamic equations in Eq. (1) as:

$$\mathcal{M}\ddot{\boldsymbol{q}} + \mathcal{K}\boldsymbol{q} = Q + \mathcal{B}\boldsymbol{z}, \tag{6}$$

where the control input matrix $\mathcal{B} \in \mathbb{R}^{n\times 8}$ corresponds to the 8 lateral vane forces in $\boldsymbol{z}$ and the generalized force matrix Q will now contain the effect of non-control external forces and moments, such as the SRP acting on the sail proper.

4. Solar sail with collocated sensors and actuators

Considering the square solar sail with two-DOF control tip vanes, it is of great advantage to assume type and placement of the sensor measurements in such a way to create a passive plant with collocated actuators and sensors. With this assumption, proportional and derivative columns of sensor measurements (output vectors) $\boldsymbol{y} \in \mathbb{R}^8$ and $\boldsymbol{y}' \in \mathbb{R}^8$ would become:

$$\begin{aligned} \boldsymbol{y} &= C\boldsymbol{q} = \mathcal{B}^T\boldsymbol{q}, \\ \boldsymbol{y}' &= C'\dot{\boldsymbol{q}} = \mathcal{B}^T\dot{\boldsymbol{q}}, \end{aligned} \tag{7}$$

where Eq. (6) is recalled and $C = \mathcal{B}^T$ and $C' = \mathcal{B}^T$ are measurement output matrices. Such a collocated passive system is advantageous since it can be stabilized with a strictly positive real controller without worrying about control and observation spillover problems [26,27] (*i.e.* destabilization due to interactions between the controller and the structural dynamics). This follows from the guaranteed passivity property (independent of the number of modes, natural frequencies, and mode shapes).

One can show that, assuming small rigid body rotations, the measurement vectors $\boldsymbol{y}$ and $\boldsymbol{y}'$ would correspond to the total translational displacements and velocities in the directions of the vanes lateral forces [20,21], *i.e.*:

$$\begin{aligned} \boldsymbol{y} &= [{}^{\mathrm{b}}p_{2,\mathrm{v1}}\ {}^{\mathrm{b}}p_{3,\mathrm{v1}}\ {}^{\mathrm{b}}p_{2,\mathrm{v2}}\ {}^{\mathrm{b}}p_{3,\mathrm{v2}}\ {}^{\mathrm{b}}p_{2,\mathrm{v3}}\ {}^{\mathrm{b}}p_{3,\mathrm{v3}}\ {}^{\mathrm{b}}p_{2,\mathrm{v4}}\ {}^{\mathrm{b}}p_{3,\mathrm{v4}}]^T, \\ \boldsymbol{y}' &= [{}^{\mathrm{b}}\dot{p}_{2,\mathrm{v1}}\ {}^{\mathrm{b}}\dot{p}_{3,\mathrm{v1}}\ {}^{\mathrm{b}}\dot{p}_{2,\mathrm{v2}}\ {}^{\mathrm{b}}\dot{p}_{3,\mathrm{v2}}\ {}^{\mathrm{b}}\dot{p}_{2,\mathrm{v3}}\ {}^{\mathrm{b}}\dot{p}_{3,\mathrm{v3}}\ {}^{\mathrm{b}}\dot{p}_{2,\mathrm{v4}}\ {}^{\mathrm{b}}\dot{p}_{3,\mathrm{v4}}]^T, \end{aligned} \tag{8}$$

where p and $\dot{p}$ represents the total translational displacement and velocity with respect to the inertial frame $\mathscr{F}_{\mathrm{I}}$ and Eq. (5) is recalled.

5. Decoupled dynamic equations using unconstrained modal coordinates

Considering Eq. (2), the finite element matrices can be partitioned and the dynamic equations of the square solar sail with control tip vanes given by Eq. (6) can be rewritten as:

$$\begin{bmatrix} \mathcal{M}_U & \mathcal{M}_{U\Theta} & \mathcal{M}_{Uu} \\ \mathcal{M}_{\Theta U} & \mathcal{M}_\Theta & \mathcal{M}_{\Theta u} \\ \mathcal{M}_{uU} & \mathcal{M}_{u\Theta} & \mathcal{M}_u \end{bmatrix} \begin{bmatrix} \ddot{\boldsymbol{U}} \\ \dot{\boldsymbol{\Omega}} \\ \ddot{\boldsymbol{u}} \end{bmatrix} + \begin{bmatrix} \mathbf{0} & \mathbf{0} & \mathbf{0} \\ \mathbf{0} & \mathbf{0} & \mathbf{0} \\ \mathbf{0} & \mathbf{0} & \mathcal{K}_u \end{bmatrix} \begin{bmatrix} \boldsymbol{U} \\ \boldsymbol{\Theta} \\ \boldsymbol{u} \end{bmatrix} = \begin{bmatrix} Q_U \\ Q_\Theta \\ Q_u \end{bmatrix} + \begin{bmatrix} \mathcal{B}_U \\ \mathcal{B}_\Theta \\ \mathcal{B}_u \end{bmatrix} \boldsymbol{z}, \tag{9}$$

where note that, since the origin of $\mathscr{F}_B$ coincides with the solar sail's center of mass, one would have $\mathcal{M}_{U\Theta} = \mathcal{M}_{\Theta U}^T = \mathbf{0}$. Also, $\mathcal{M}_U = m\mathbf{1}$ and $\mathcal{M}_\Theta = \boldsymbol{J}$ where m is the total mass (translational inertia) of the solar sail and $\boldsymbol{J}$ is its total rotational inertia about the center of mass. One can show that $Q_U + \mathcal{B}_U \boldsymbol{z}$ and $Q_\Theta + \mathcal{B}_\Theta \boldsymbol{z}$ accordingly are the net (summation of control and non-control) external forces and moments applied to the solar sail [20,21]. Analogous to the dynamic equations, the collocated measurements $\boldsymbol{y}$ and $\boldsymbol{y}'$ can be rewritten as:

$$\begin{aligned} \boldsymbol{y} &= \mathcal{B}^T \boldsymbol{q} = [\mathcal{B}_U^T \;\; \mathcal{B}_\Theta^T \;\; \mathcal{B}_u^T][\boldsymbol{U}^T \;\; \boldsymbol{\Theta}^T \;\; \boldsymbol{u}^T]^T, \\ \boldsymbol{y}' &= \mathcal{B}^T \dot{\boldsymbol{q}} = [\mathcal{B}_U^T \;\; \mathcal{B}_\Theta^T \;\; \mathcal{B}_u^T][\dot{\boldsymbol{U}}^T \;\; \boldsymbol{\Omega}^T \;\; \dot{\boldsymbol{u}}^T]^T. \end{aligned} \tag{10}$$

Now the matrix of unconstrained non-rigid mode shapes of the solar sail $\mathcal{S} \in \mathbb{R}^{n\times(n-6)}$ (each column of $\mathcal{S}$ represents a non-rigid unconstrained mode shape), partitioned as:

$$\mathcal{S} = [\mathcal{S}_U^T \;\; \mathcal{S}_\Theta^T \;\; \mathcal{S}_u^T]^T, \tag{11}$$

can be used to define a transformation of the form:

$$\ddot{\boldsymbol{q}} = \mathcal{T}\ddot{\hat{\boldsymbol{q}}}, \qquad \dot{\boldsymbol{q}} = \mathcal{T}\dot{\hat{\boldsymbol{q}}}, \qquad \boldsymbol{q} = \mathcal{T}\hat{\boldsymbol{q}}, \tag{12}$$

where:

$$\mathcal{T} = \begin{bmatrix} \boldsymbol{1} & \mathbf{0} & \mathcal{S}_U \\ \mathbf{0} & \boldsymbol{1} & \mathcal{S}_\Theta \\ \mathbf{0} & \mathbf{0} & \mathcal{S}_u \end{bmatrix},$$

$$\ddot{\hat{\boldsymbol{q}}} = \begin{bmatrix} \ddot{\hat{\boldsymbol{U}}} \\ \dot{\hat{\boldsymbol{\Omega}}} \\ \ddot{\hat{\boldsymbol{u}}} \end{bmatrix}, \qquad \dot{\hat{\boldsymbol{q}}} = \begin{bmatrix} \dot{\hat{\boldsymbol{U}}} \\ \hat{\boldsymbol{\Omega}} \\ \dot{\hat{\boldsymbol{u}}} \end{bmatrix}, \qquad \hat{\boldsymbol{q}} = \begin{bmatrix} \hat{\boldsymbol{U}} \\ \hat{\boldsymbol{\Theta}} \\ \hat{\boldsymbol{u}} \end{bmatrix}, \tag{13}$$

and decouple the dynamic equations of the solar sail to express them in terms of the unconstrained modal coordinates as [20,21,28]:

$$\begin{bmatrix} \mathcal{M}_U & \mathbf{0} & \mathbf{0} \\ \mathbf{0} & \mathcal{M}_\Theta & \mathbf{0} \\ \mathbf{0} & \mathbf{0} & \boldsymbol{1} \end{bmatrix} \begin{bmatrix} \ddot{\hat{\boldsymbol{U}}} \\ \dot{\hat{\boldsymbol{\Omega}}} \\ \ddot{\hat{\boldsymbol{u}}} \end{bmatrix} + \begin{bmatrix} \mathbf{0} & \mathbf{0} & \mathbf{0} \\ \mathbf{0} & \mathbf{0} & \mathbf{0} \\ \mathbf{0} & \mathbf{0} & \omega^2 \end{bmatrix} \begin{bmatrix} \hat{\boldsymbol{U}} \\ \hat{\boldsymbol{\Theta}} \\ \hat{\boldsymbol{u}} \end{bmatrix} = \begin{bmatrix} Q_U \\ Q_\Theta \\ \hat{Q}_u \end{bmatrix} + \begin{bmatrix} \mathcal{B}_U \\ \mathcal{B}_\Theta \\ \hat{\mathcal{B}}_u \end{bmatrix} \boldsymbol{z}, \tag{14}$$

or:

$$\begin{aligned} \mathcal{M}_U \ddot{\hat{\boldsymbol{U}}} &= Q_U + \mathcal{B}_U \boldsymbol{z}, \\ \mathcal{M}_\Theta \dot{\hat{\boldsymbol{\Omega}}} &= Q_\Theta + \mathcal{B}_\Theta \boldsymbol{z}, \\ \ddot{\hat{\boldsymbol{u}}} + \omega^2 \hat{\boldsymbol{u}} &= \hat{Q}_u + \hat{\mathcal{B}}_u \boldsymbol{z}, \end{aligned} \tag{15}$$

where ω is the diagonal matrix of $n-6$ non-zero unconstrained natural frequencies and:

$$\begin{aligned} \hat{Q}_u &= \mathcal{S}^T Q, \\ \hat{\mathcal{B}}_u &= \mathcal{S}^T \mathcal{B}. \end{aligned} \tag{16}$$

It is also useful to use Eqs. (12) and (13) and rewrite the collocated measurement vectors $\boldsymbol{y}$ and $\boldsymbol{y}'$, given by Eq. (10), as:

$$\begin{aligned} \boldsymbol{y} &= \mathcal{B}^T \mathcal{T} \hat{\boldsymbol{q}} = [\mathcal{B}_U^T \;\; \mathcal{B}_\Theta^T \;\; \hat{\mathcal{B}}_u] \hat{\boldsymbol{q}}, \\ \boldsymbol{y}' &= \mathcal{B}^T \mathcal{T} \dot{\hat{\boldsymbol{q}}} = [\mathcal{B}_U^T \;\; \mathcal{B}_\Theta^T \;\; \hat{\mathcal{B}}_u] \dot{\hat{\boldsymbol{q}}}, \end{aligned} \tag{17}$$

where the second relation in Eq. (16) is recalled.

6. Collocated attitude controller

The collocated attitude controller (without vibrations control) developed in Ref. [12] is summarized in this section and will be used as a reference to compare other controllers that will be presented in this study against it. By using $\boldsymbol{y}$ and $\boldsymbol{y}'$ defined in Eqs. (7) and (8), the solar sail overall (average) attitude and rotational velocity $\bar{\boldsymbol{\Theta}} \in \mathbb{R}^3$ and $\bar{\boldsymbol{\Omega}} \in \mathbb{R}^3$ can be defined as [12]:

$$\begin{aligned} \bar{\boldsymbol{\Theta}} &= \boldsymbol{R}\boldsymbol{y} = \boldsymbol{R}\mathcal{B}^T \boldsymbol{q}, \\ \bar{\boldsymbol{\Omega}} &= \boldsymbol{R}\boldsymbol{y}' = \boldsymbol{R}\mathcal{B}^T \dot{\boldsymbol{q}}, \end{aligned} \tag{18}$$

where $\boldsymbol{R}$ is the translational to rotational coordinates conversion matrix:

$$\boldsymbol{R} = \frac{1}{4L_b} \begin{bmatrix} 0 & 0 & 0 & 2 & 0 & 0 & 0 & -2 \\ 0 & -2 & 0 & 0 & 0 & 2 & 0 & 0 \\ 1 & 0 & 1 & 0 & 1 & 0 & 1 & 0 \end{bmatrix}. \tag{19}$$

Now a proportional-derivative (PD) control law with positive scalar coefficients k and k' may be defined to calculate the required control torque $\boldsymbol{T}_c \in \mathbb{R}^3$ as:

$$\boldsymbol{T}_c = -k\bar{\boldsymbol{\Theta}} - k'\bar{\boldsymbol{\Omega}} = -k\boldsymbol{R}\boldsymbol{y} - k'\boldsymbol{R}\boldsymbol{y}', \qquad k > 0,\ k' > 0, \tag{20}$$

which is used to derive the control input vector $\boldsymbol{z}$ (including the vanes lateral control forces) from:

$$\boldsymbol{z} = \boldsymbol{F}\boldsymbol{T}_c, \tag{21}$$

where $\boldsymbol{F}$ is the torque to force conversion matrix and one can show that $\boldsymbol{F} = \boldsymbol{R}^T$.

By combining Eqs. (18), (20) and (21) with Eq. (6), the combined dynamic equations of the solar sail and the attitude controller can be written as:

$$\mathcal{M}\ddot{\boldsymbol{q}} + \mathcal{B}\boldsymbol{R}^T k' \boldsymbol{R}\mathcal{B}^T \dot{\boldsymbol{q}} + (\mathcal{K} + \mathcal{B}\boldsymbol{R}^T k \boldsymbol{R}\mathcal{B}^T)\boldsymbol{q} = Q, \tag{22}$$

where we note that matrices $\mathcal{B}\boldsymbol{R}^T k \boldsymbol{R}\mathcal{B}^T$ and $\mathcal{B}\boldsymbol{R}^T k' \boldsymbol{R}\mathcal{B}^T$ are symmetric and positive semi-definite. One can conclude that the collocated attitude controller is only adding positive stiffness and (active) damping effects to some of the elastic modes of the solar sail and may not destabilize the spacecraft. Such a controller would not result in any spillover issues.

It is noteworthy that $\boldsymbol{R}\boldsymbol{y}$ contains contributions from the rigid body rotations at the solar sail center and from some of the elastic modes. Therefore, for large rigid body rotations and attitude tracking control purposes, one may replace the contribution of rigid body rotations with twice the vector part of the attitude error quaternion, *i.e.* $2\varepsilon_e$ [12]. The attitude error quaternion is calculated from the desired orientation quaternion $\{\varepsilon_d, \eta_d\}$ and the current orientation quaternion $\{\varepsilon, \eta\}$ as:

$$\begin{bmatrix} \varepsilon_e \\ \eta_e \end{bmatrix} = \begin{bmatrix} \eta_d 1 - \varepsilon_d^\times & -\varepsilon_d \\ \varepsilon_d^T & \eta_d \end{bmatrix} \begin{bmatrix} \varepsilon \\ \eta \end{bmatrix}. \tag{23}$$

7. Collocated attitude and vibrations controller

Before talking about the collocated attitude and vibrations control, it is worth mentioning that the goal of the vibrations control is to suppress or damp out the dynamic vibrations of the solar sail and not to reduce its static elastic deformations. The control vanes are not intended (nor are capable) to eliminate the solar sail deflections due to the SRP. Therefore, it would be more appropriate to only feedback the elastic velocities (and not the elastic displacements) for the purpose of the vibrations control.

Also, note that for attitude and vibrations controls, it is necessary to somehow exclude the effect of continuously-growing rigid body translational displacements and velocities $\boldsymbol{U}$ and $\dot{\boldsymbol{U}}$ from the collocated

measurements $\boldsymbol{y}$ and $\boldsymbol{y}'$. However, doing such without violating the passivity of the solar sail (achieved by collocated sensors and actuators) is not very straightforward. This was done automatically for the collocated attitude controller developed in the previous section by multiplying measurements $\boldsymbol{y}$ and $\boldsymbol{y}'$ by matrix $\boldsymbol{R}$ before feeding them back to the PD attitude controller.

7.1. First approach

A first simple solution to these problems could be to combine the proportional part of the collocated PD attitude controller developed in the previous section with a derivative attitude and vibrations controller which is based on a modified derivative measurement $\tilde{\boldsymbol{y}}'$ of the form:

$$\tilde{\boldsymbol{y}}' = \boldsymbol{y}' - \mathcal{B}_U^T\dot{\boldsymbol{U}} = \mathcal{B}^T\dot{\boldsymbol{q}} - [\mathcal{B}_U^T \;\; \boldsymbol{0} \;\; \boldsymbol{0}]\dot{\boldsymbol{q}} = [\boldsymbol{0} \;\; \mathcal{B}_\Theta^T \;\; \mathcal{B}_{\boldsymbol{u}}^T]\dot{\boldsymbol{q}} = \tilde{\mathcal{B}}^T\dot{\boldsymbol{q}}, \tag{24}$$

where now, in addition to $\boldsymbol{y}$ and $\boldsymbol{y}'$, it is also required to measure the translational velocity $\dot{\boldsymbol{U}}$ at the solar sail's hub. The final PD attitude and vibrations controller would then take the form:

$$\boldsymbol{z} = -\boldsymbol{R}^T k\boldsymbol{R}\boldsymbol{y} - k'\tilde{\boldsymbol{y}}', \qquad k > 0,\ k' > 0. \tag{25}$$

Incorporating such a controller with the dynamic equations of the solar sail in Eq. (6) results in:

$$\mathcal{M}\ddot{\boldsymbol{q}} + \mathcal{B}k'\tilde{\mathcal{B}}^T\dot{\boldsymbol{q}} + (\mathcal{K} + \mathcal{B}\boldsymbol{R}^T k\boldsymbol{R}\mathcal{B}^T)\boldsymbol{q} = \mathcal{Q}, \tag{26}$$

where now despite $\mathcal{B}\boldsymbol{R}^T k\boldsymbol{R}\mathcal{B}^T$ being symmetric and positive semi-definite, the matrix $\mathcal{B}k'\tilde{\mathcal{B}}^T$ is not symmetric and is not guaranteed to have a positive semi-definite symmetric part. Therefore, it may potentially destabilize the solar sail spacecraft (spillover destabilization may occur).

For a closer investigation, one can show that $\mathcal{B}_U\mathcal{B}_\Theta^T = \mathcal{B}_\Theta\mathcal{B}_U^T = \boldsymbol{0}$ and then write $\mathcal{B}k'\tilde{\mathcal{B}}^T$ as:

$$\mathcal{B}k'\tilde{\mathcal{B}}^T = k'\mathcal{B}\tilde{\mathcal{B}}^T = k'\begin{bmatrix}\mathcal{B}_U\\ \mathcal{B}_\Theta\\ \mathcal{B}_{\boldsymbol{u}}\end{bmatrix}[\boldsymbol{0} \;\; \mathcal{B}_\Theta^T \;\; \mathcal{B}_{\boldsymbol{u}}^T] = k'\begin{bmatrix}\boldsymbol{0} & \boldsymbol{0} & \mathcal{B}_U\mathcal{B}_{\boldsymbol{u}}^T\\ \boldsymbol{0} & \mathcal{B}_\Theta\mathcal{B}_\Theta^T & \mathcal{B}_\Theta\mathcal{B}_{\boldsymbol{u}}^T\\ \boldsymbol{0} & \mathcal{B}_{\boldsymbol{u}}\mathcal{B}_\Theta^T & \mathcal{B}_{\boldsymbol{u}}\mathcal{B}_{\boldsymbol{u}}^T\end{bmatrix}, \tag{27}$$

which can be decomposed into symmetric and skew-symmetric parts as:

$$\mathcal{B}k'\tilde{\mathcal{B}}^T = k'\begin{bmatrix}\frac{1}{2}\mathcal{B}_U\\ \mathcal{B}_\Theta\\ \mathcal{B}_{\boldsymbol{u}}\end{bmatrix}\begin{bmatrix}\frac{1}{2}\mathcal{B}_U^T & \mathcal{B}_\Theta^T & \mathcal{B}_{\boldsymbol{u}}^T\end{bmatrix} + k'\begin{bmatrix}-\frac{1}{4}\mathcal{B}_U\mathcal{B}_U^T & \boldsymbol{0} & \boldsymbol{0}\\ \boldsymbol{0} & \boldsymbol{0} & \boldsymbol{0}\\ \boldsymbol{0} & \boldsymbol{0} & \boldsymbol{0}\end{bmatrix} + k'\begin{bmatrix}\boldsymbol{0} & \boldsymbol{0} & \frac{1}{2}\mathcal{B}_U\mathcal{B}_{\boldsymbol{u}}^T\\ \boldsymbol{0} & \boldsymbol{0} & \boldsymbol{0}\\ -\frac{1}{2}\mathcal{B}_{\boldsymbol{u}}\mathcal{B}_U^T & \boldsymbol{0} & \boldsymbol{0}\end{bmatrix}. \tag{28}$$

Recalling that $k' > 0$, one may notice in Eq. (28) that the first term is a symmetric positive semi-definite matrix, the second term is a symmetric negative semi-definite matrix, and the third term is a skew-symmetric matrix. Therefore, on top of adding some positive damping effects and some (irrelevant) coupling effects, the matrix $\mathcal{B}k'\tilde{\mathcal{B}}^T$ would be contributing vital negative damping effects (because of the second term) to the trajectory dynamics of the solar sail associated with $\boldsymbol{U}$. If not accounted for by the trajectory controller, these negative damping effects (although very small) can potentially destabilize the trajectory dynamics of the solar sail spacecraft. This case can be interpreted as having control spillover from the controlled modes associated with $\boldsymbol{\Theta}$ and $\boldsymbol{u}$ to the uncontrolled modes corresponding to $\boldsymbol{U}$ and also having observation spillover from the uncontrolled modes to the measurements of the controlled modes and, therefore, facing potential spillover destabilization [26,27].

7.2. Second approach

A second safer approach towards solving the collocated attitude and vibrations control problem could be to establish the controller using the decoupled dynamic equations in Eq. (14) or (15). Note that solar sail trajectory control by using the effect of SRP on the main sails is done indirectly through the attitude and vibrations controls. The control vanes are not intended to nor are capable to do any trajectory control and, considering their total surface area relative to the main sails (at around 2%), the net force generated by vanes would have a small (disturbance-like) effect on the overall trajectory of the solar sail. Therefore, it is conceivable and probably wiser to isolate the trajectory dynamics of the solar sail from its attitude and flexible dynamics and focus on the latter when devising the attitude and vibrations control law to calculate the required vane forces. The decoupled dynamic equations in Eq. (14) or (15) would allow for such a separation to be performed.

Recalling Eq. (14) or (15), the separated dynamic equations of the solar sail may be written as:

$$\begin{aligned}&\mathcal{M}_U\ddot{\hat{\boldsymbol{U}}} = \mathcal{Q}_U + \mathcal{B}_U\boldsymbol{z},\\ &\begin{bmatrix}\mathcal{M}_\Theta & \boldsymbol{0}\\ \boldsymbol{0} & \boldsymbol{1}\end{bmatrix}\begin{bmatrix}\dot{\hat{\boldsymbol{\Omega}}}\\ \ddot{\hat{\boldsymbol{u}}}\end{bmatrix} + \begin{bmatrix}\boldsymbol{0} & \boldsymbol{0}\\ \boldsymbol{0} & \omega^2\end{bmatrix}\begin{bmatrix}\hat{\boldsymbol{\Theta}}\\ \hat{\boldsymbol{u}}\end{bmatrix} = \begin{bmatrix}\mathcal{Q}_\Theta\\ \hat{\mathcal{Q}}_{\boldsymbol{u}}\end{bmatrix} + \begin{bmatrix}\mathcal{B}_\Theta\\ \hat{\mathcal{B}}_{\boldsymbol{u}}\end{bmatrix}\boldsymbol{z}.\end{aligned} \tag{29}$$

Now a set of measurements $\tilde{\boldsymbol{y}}$ and $\tilde{\boldsymbol{y}}'$ defined as:

$$\begin{aligned}\tilde{\boldsymbol{y}} &= \begin{bmatrix}\mathcal{B}_\Theta^T & \hat{\mathcal{B}}_{\boldsymbol{u}}^T\end{bmatrix}\begin{bmatrix}\hat{\boldsymbol{\Theta}}\\ \hat{\boldsymbol{u}}\end{bmatrix} = \tilde{\mathcal{B}}^T\begin{bmatrix}\hat{\boldsymbol{\Theta}}\\ \hat{\boldsymbol{u}}\end{bmatrix},\\ \tilde{\boldsymbol{y}}' &= \begin{bmatrix}\mathcal{B}_\Theta^T & \hat{\mathcal{B}}_{\boldsymbol{u}}^T\end{bmatrix}\begin{bmatrix}\hat{\boldsymbol{\Omega}}\\ \dot{\hat{\boldsymbol{u}}}\end{bmatrix} = \tilde{\mathcal{B}}^T\begin{bmatrix}\hat{\boldsymbol{\Omega}}\\ \dot{\hat{\boldsymbol{u}}}\end{bmatrix},\end{aligned} \tag{30}$$

can be used within a PD control law:

$$\boldsymbol{z} = -\boldsymbol{R}^T k\boldsymbol{R}\tilde{\boldsymbol{y}} - k'\tilde{\boldsymbol{y}}', \qquad k > 0,\ k' > 0, \tag{31}$$

to rewrite the dynamic equations in Eq. (29) as:

$$\begin{aligned}&\mathcal{M}_U\ddot{\hat{\boldsymbol{U}}} = \mathcal{Q}_U - k'\mathcal{B}_U\hat{\mathcal{B}}_{\boldsymbol{u}}^T\dot{\hat{\boldsymbol{u}}},\\ &\begin{bmatrix}\mathcal{M}_\Theta & \boldsymbol{0}\\ \boldsymbol{0} & \boldsymbol{1}\end{bmatrix}\begin{bmatrix}\dot{\hat{\boldsymbol{\Omega}}}\\ \ddot{\hat{\boldsymbol{u}}}\end{bmatrix} + \tilde{\mathcal{B}}k'\tilde{\mathcal{B}}^T\begin{bmatrix}\hat{\boldsymbol{\Omega}}\\ \dot{\hat{\boldsymbol{u}}}\end{bmatrix} + \left(\begin{bmatrix}\boldsymbol{0} & \boldsymbol{0}\\ \boldsymbol{0} & \omega^2\end{bmatrix} + \tilde{\mathcal{B}}\boldsymbol{R}^T k\boldsymbol{R}\tilde{\mathbf{B}}^T\right)\begin{bmatrix}\hat{\boldsymbol{\Theta}}\\ \hat{\boldsymbol{u}}\end{bmatrix} = \begin{bmatrix}\mathcal{Q}_\Theta\\ \hat{\mathcal{Q}}_{\boldsymbol{u}}\end{bmatrix},\end{aligned} \tag{32}$$

where one can show that $\mathcal{B}_U\boldsymbol{R}^T = \boldsymbol{0}$ and $\mathcal{B}_U\mathcal{B}_\Theta^T = \boldsymbol{0}$ and therefore:

$$\begin{aligned}&\mathcal{B}_U\boldsymbol{R}^T k\boldsymbol{R}\tilde{\mathbf{B}}^T = \boldsymbol{0},\\ &\mathcal{B}_U\tilde{\mathbf{B}}^T = \mathcal{B}_U\begin{bmatrix}\mathcal{B}_\Theta^T & \hat{\mathcal{B}}_{\boldsymbol{u}}^T\end{bmatrix} = \begin{bmatrix}0 & \mathcal{B}_U\hat{\mathcal{B}}_{\boldsymbol{u}}^T\end{bmatrix}.\end{aligned} \tag{33}$$

In Eq. (32), the matrices $\tilde{\mathcal{B}}\boldsymbol{R}^T k\boldsymbol{R}\tilde{\mathbf{B}}^T$ and $\tilde{\mathcal{B}}k'\tilde{\mathcal{B}}^T$ are symmetric and positive semi-definite and would not destabilize the attitude or flexible dynamics of the solar sail. One may interpret this case as having control spillover from the controlled modes associated with $\hat{\boldsymbol{\Theta}}$ and $\hat{\boldsymbol{u}}$ to the uncontrolled modes corresponding to $\hat{\boldsymbol{U}}$ but having no observation spillover from the uncontrolled modes to the measurements of controlled modes (and therefore facing no spillover destabilization [26,27]).

As part of its task, the trajectory controller should be responsible to account for the control spillover to the trajectory dynamics, *i.e.* to cancel out the disturbance-like term $k'\mathcal{B}_U\hat{\mathcal{B}}_{\boldsymbol{u}}^T\dot{\hat{\boldsymbol{u}}}$ in the solar sail's trajectory dynamic equations given by the first relation of Eq. (32). It is worth mentioning that the control spillover term is actually the net force generated by the four control vanes, *i.e.*:

$$k'\mathcal{B}_U\hat{\mathcal{B}}_{\boldsymbol{u}}^T\dot{\hat{\boldsymbol{u}}} = \boldsymbol{f}_{\mathrm{v1}} + \boldsymbol{f}_{\mathrm{v2}} + \boldsymbol{f}_{\mathrm{v3}} + \boldsymbol{f}_{\mathrm{v4}}, \tag{34}$$

where $\boldsymbol{f}_{\mathrm{v}}$ is the vane force vector described in $\mathscr{F}_{\mathrm{B}}$.

The only concern about the proposed collocated controller would be constructing the measurements $\tilde{\boldsymbol{y}}$ and $\tilde{\boldsymbol{y}}'$ in Eq. (30) from the collocated measurements $\boldsymbol{y}$ and $\boldsymbol{y}'$ and some other measurable (physical) or estimable variables. To achieve this, one may note that $\boldsymbol{R}\mathcal{B}_U^T = \boldsymbol{0}$ and therefore:

$$\boldsymbol{R}\tilde{\boldsymbol{y}} = \boldsymbol{R}\begin{bmatrix}\boldsymbol{0} & \mathcal{B}_{\Theta}^{T} & \hat{\mathcal{B}}_{\boldsymbol{u}}^{T}\end{bmatrix}\begin{bmatrix}\hat{\boldsymbol{U}}\\ \hat{\boldsymbol{\Theta}}\\ \hat{\boldsymbol{u}}\end{bmatrix} = \boldsymbol{R}\begin{bmatrix}\mathcal{B}_{U}^{T} & \mathcal{B}_{\Theta}^{T} & \hat{\mathcal{B}}_{\boldsymbol{u}}^{T}\end{bmatrix}\begin{bmatrix}\hat{\boldsymbol{U}}\\ \hat{\boldsymbol{\Theta}}\\ \hat{\boldsymbol{u}}\end{bmatrix} = \boldsymbol{R}\boldsymbol{y}, \tag{35}$$

where Eq. (17) is recalled. Also one may rewrite the second relation of Eq. (30) as:

$$\tilde{\boldsymbol{y}}' = \begin{bmatrix}\boldsymbol{0} & \mathcal{B}_{\Theta}^{T} & \hat{\mathcal{B}}_{\boldsymbol{u}}^{T}\end{bmatrix}\begin{bmatrix}\dot{\hat{\boldsymbol{U}}}\\ \dot{\hat{\boldsymbol{\Omega}}}\\ \dot{\hat{\boldsymbol{u}}}\end{bmatrix} = \begin{bmatrix}\mathcal{B}_{U}^{T} & \mathcal{B}_{\Theta}^{T} & \hat{\mathcal{B}}_{\boldsymbol{u}}^{T}\end{bmatrix}\dot{\hat{\boldsymbol{q}}} - \mathcal{B}_{U}^{T}\dot{\hat{\boldsymbol{U}}} = \boldsymbol{y}' - \mathcal{B}_{U}^{T}\dot{\hat{\mathbf{U}}}, \tag{36}$$

where Eq. (17) is recalled again and note that $\mathcal{B}_U$ is a known 8×3 matrix. Thus, it is only required to measure or estimate $\dot{\hat{\boldsymbol{U}}}$.

One solution to this problem is to numerically integrate the trajectory dynamic equation, *i.e.* the first relation of Eq. (32) and calculate an estimation of $\dot{\hat{\boldsymbol{U}}}$. For another solution, consider the linear nature of the trajectory dynamic equation in Eq. (32), recall Eq. (34), and write:

$$\begin{aligned}\dot{\hat{\boldsymbol{U}}} &= \dot{\hat{\boldsymbol{U}}}_1 + \dot{\hat{\boldsymbol{U}}}_2,\\ \ddot{\hat{\boldsymbol{U}}} &= \ddot{\hat{\boldsymbol{U}}}_1 + \ddot{\hat{\boldsymbol{U}}}_2,\end{aligned} \tag{37}$$

where:

$$\begin{aligned}\mathcal{M}_U\ddot{\hat{\boldsymbol{U}}}_1 &= Q_U,\\ \mathcal{M}_U\ddot{\hat{\boldsymbol{U}}}_2 &= \boldsymbol{f}_{v1} + \boldsymbol{f}_{v2} + \boldsymbol{f}_{v3} + \boldsymbol{f}_{v4},\end{aligned} \tag{38}$$

The first relation in Eq. (38) is driven by the low-frequency force Q_U from the SRP on the main sails and the second relation is driven by vane forces. One can conclude that applying a low pass filter to the translational velocity measurements at the solar sail's hub, *i.e.* $\dot{\boldsymbol{U}}$, would result in $\dot{\hat{\boldsymbol{U}}}_1$. Then $\dot{\hat{\boldsymbol{U}}}_2$ can be estimated by integrating the second relation of Eq. (38).

8. Numerical results

Numerical examples based on a case study solar sail will be provided in this section to examine the performance of the developed attitude and vibrations controllers and study their interactions with the structural dynamics of the solar sail.

8.1. Case study: 150 m square solar sail

As a case study, consider the 150 m five-point connected square solar sail studied in Refs. [12,13]. The solar sail is composed of four booms and four triangular sail quadrants which are connected at five points, *i.e.* at the central hub and at the tip ends of booms. The booms are thin-walled tubes of radius 0.229 m, thickness 7.5 μm, and length $150/\sqrt{2}$ m. The sail quadrants are right-angled isosceles triangular membranes of thickness 2.5 μm and side length $150/\sqrt{2}$ m. Each sail quadrant is pre-tensioned by applying concentrated forces at its three vertices. These forces are such that the von Mises stress at the triangular quadrant centroid is 6895 Pa (1 psi) and the sail quadrant is in static equilibrium (each force line of action passes through triangular quadrant centroid).

A 291.05 kg concentrated mass, representing the central bus, control mast, payload, and other equipment and instrumentation, is located at the center of the solar sail. The moments of inertia associated with this concentrated mass are assumed to be 1014.35 $\mathrm{kg \cdot m^2}$, 1014.35 $\mathrm{kg \cdot m^2}$, and 36.56 $\mathrm{kg \cdot m^2}$ respectively about the x_1, x_2, and x_3 axes of the body frame $\mathcal{F}_B$. A 0.58 kg concentrated mass representing a control tip vane is also located at the tip end of each boom. The tip vanes are assumed to be double-sided reflective right isosceles triangles with a side length of 15 m, each having two angular DOFs with respect to its supporting boom. The other parameters needed by the linear structural model developed in the previous section are calculated and listed in Table 1 [12,13].

Table 1
Summary of the square solar sail model parameters.

Each of the 4 Triangular Sails		Each of the 4 Booms	
Side length	$150/\sqrt{2}$ m	Length	$150/\sqrt{2}$ m
Surface area	$5625\mathrm{m^2}$	Cross-sectional area	$1.08 \times 10^{-5}\mathrm{m^2}$
Thickness	2.50×10^{-6} m	Second moment of area	$2.83 \times 10^{-7}\mathrm{m^4}$
Density	$1572\mathrm{kg\ m^3}$	Density	$1908\mathrm{kg\ m^3}$
Young's modulus	2.48×10^{9} Pa	Young's modulus	124×10^{9} Pa
Poisson's ratio	0.34	Poisson's ratio	0.30

For such a solar sail, the FEM-based linear structural model, summarized previously, is used to derive discretized linear dynamic equations in a linear matrix-second-order form as given by Eq. (6). Each boom is divided into 30 linear elements (31 nodes) and each sail is meshed with 900 triangular elements (496 nodes).

8.2. Attitude control maneuver

To illustrate the performance of the developed collocated attitude and vibrations controllers, an attitude maneuver will be presented in this section. In the maneuver, the 150 m square solar sail, initially undeformed and at rest, is exposed to a SRP of 4.56 $\mu\mathrm{m/m^2}$ (formulated using the linear photonic thrust model [29]) that is perpendicular to its surface at $t = 0s$. The solar sail starts from this orientation with x_1 - x_2 - x_3 Euler angles of $\theta_1 = \theta_2 = \theta_3 = 0$ and it is desired to rotate the sail to a final orientation where $\theta_1 = \frac{\pi}{3}$, $\theta_2 = -\frac{\pi}{3}$, and $\theta_3 = -\frac{\pi}{4}$. The desired orientation is given to the controller as a step input (without any input shaping). The two-variable optimization problem, given by Eq. (4) and required to determine the vane angles, is solved by using a particle swarm optimization algorithm toolbox [30]. Although being a meta-heuristic algorithm that can not guarantee an optimal solution, the particle swarm optimization is usually known to be effective and fast in finding the global optimum solution for nonlinear optimization problems with a confined search domain [30]. The controller coefficients are chosen to be $k = 5\mathrm{N{\cdot}m}$ and $k' = 2500\mathrm{N{\cdot}m{\cdot}s/rad}$ and the optimization weighting coefficients are set to be $w_1 = w_2 = \frac{1}{2}$.

Employing the three attitude and vibrations controllers, presented in the previous sections, the control vane angles and the dynamic response of the solar sail during the considered attitude maneuver are plotted in Figs. 4–6. The results are obtained using the FEM-based linear structural model of the solar sail.

Plots of Fig. 4 illustrate the performance of the collocated attitude controller. Although the controller proves to be capable of rotating the solar sail to the desired orientation, one may notice the persistence of the spacecraft's structural vibrations. Plots of Figs. 5 and 6 represent the performances of the two collocated attitude and vibrations controllers (developed by taking the first and the second approaches explained in the previous section). Notice that both controllers prove to be capable of simultaneous attitude and vibrations controls. In particular, the first attitude and vibrations controller suppresses the elastic vibrations slightly faster. Note that, as expected, for vibrations control (vibrations suppression) it is necessary to rotate the vanes relatively faster than the case of pure attitude control. This is clear by comparing the first two plots of Figs. 5 and 6 to the first two plots of Fig. 4. Such fast-responding control vanes, however, may not be feasible in practice and one may question the vibrations controlling performance of the developed controllers. Nevertheless, as far as the structural dynamics of the solar sail is considered, one may note that none of the three developed controllers may destabilize the solar sail. Although the first attitude and vibrations controller can potentially destabilize the trajectory dynamics of the solar sail, this is not the case at least for the considered attitude maneuver and during the considered time frame. This potential

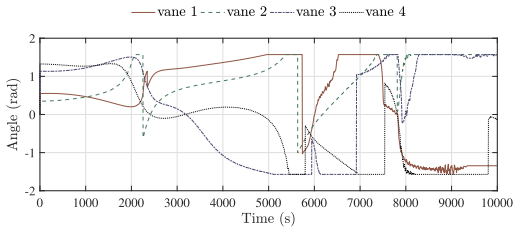

(a) First angular DOF of control vanes (α_1)

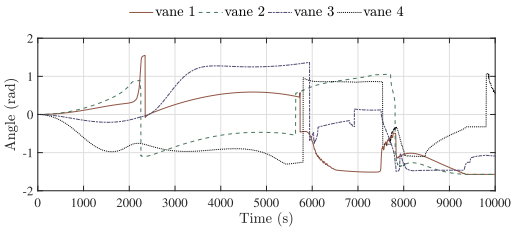

(b) Second angular DOF of control vanes (α_2)

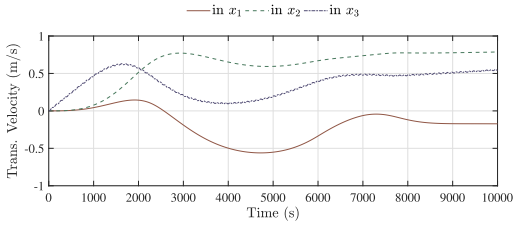

(c) Translational velocities at the center

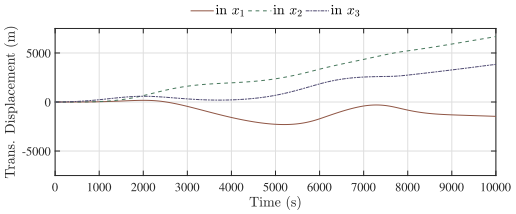

(d) Translational displacements at the center

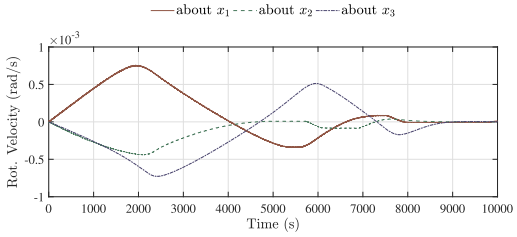

(e) Rotational velocities at the center

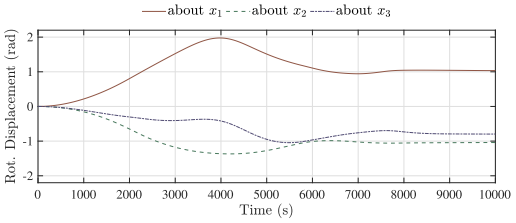

(f) Rotational displacements (Euler angles) at the center

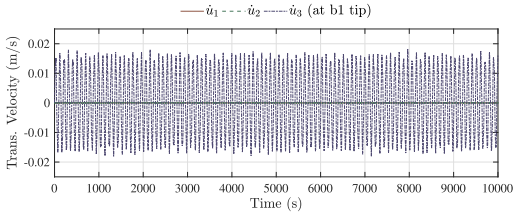

(g) Translational velocities at the tip of boom 1 (b1)

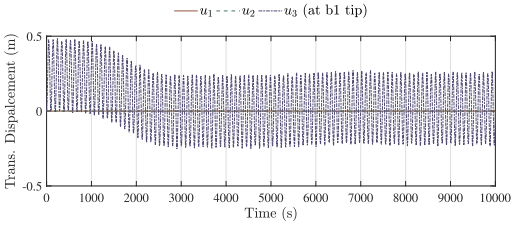

(h) Translational displacements at the tip of boom 1 (b1)

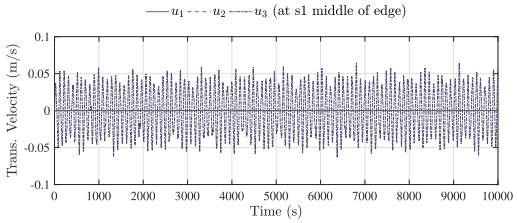

(i) Trans. velocities at the middle edge of sail 1 (s1)

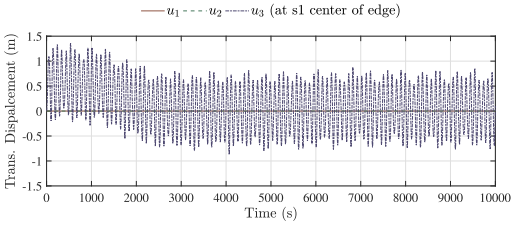

(j) Trans. displacements at the middle edge of sail 1 (s1)

Fig. 4. Solar sail dynamics with a collocated attitude controller (represented in $\mathcal{F}_B$) during the attitude maneuver from $\theta_1 = \theta_2 = \theta_3 = 0$ to $\theta_1 = \frac{\pi}{3}$, $\theta_2 = -\frac{\pi}{3}$, $\theta_3 = -\frac{\pi}{4}$.

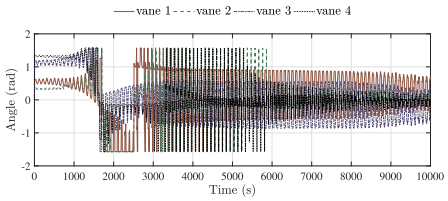

(a) First angular DOF of control vanes (α_1)

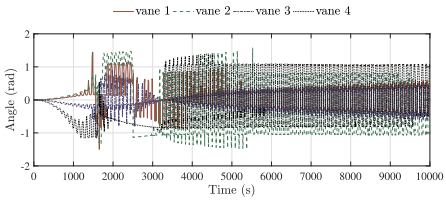

(b) Second angular DOF of control vanes (α_2)

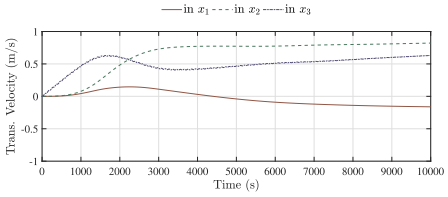

(c) Translational velocities at the center

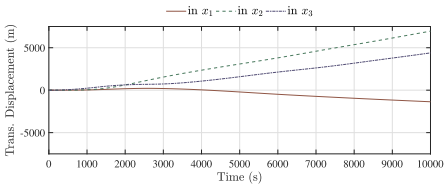

(d) Translational displacements at the center

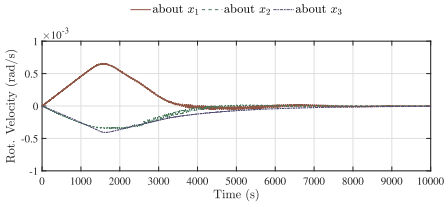

(e) Rotational velocities at the center

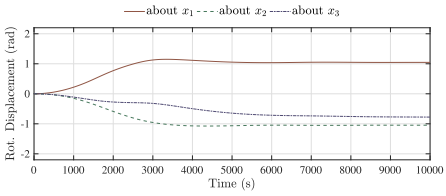

(f) Rotational displacements (Euler angles) at the center

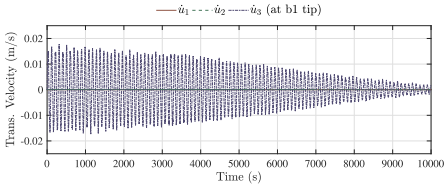

(g) Translational velocities at the tip of boom 1 (b1)

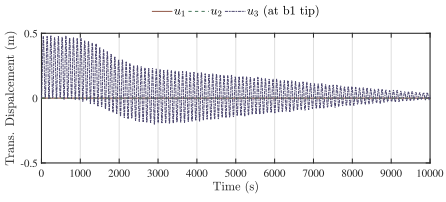

(h) Translational displacements at the tip of boom 1 (b1)

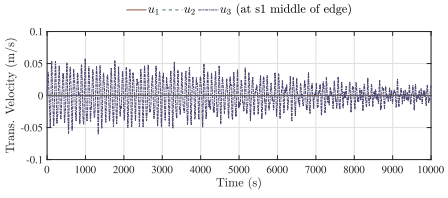

(i) Trans. velocities at the middle edge of sail 1 (s1)

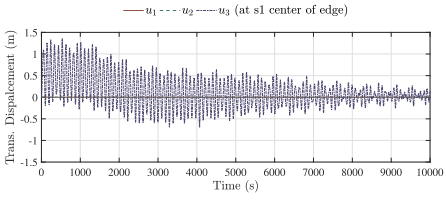

(j) Trans. displacements at the middle edge of sail 1 (s1)

Fig. 5. Solar sail dynamics with the first collocated attitude and vibrations controller (represented in $\mathcal{F}_B$) during the attitude maneuver from $\theta_1 = \theta_2 = \theta_3 = 0$ to $\theta_1 = \frac{\pi}{3}$, $\theta_2 = -\frac{\pi}{3}$, $\theta_3 = -\frac{\pi}{4}$.

destabilization may become more important when a trajectory controller is incorporated to the dynamics of the solar sail. Investigating such a case would be left to a future work.

9. Conclusion

Attitude and vibrations controls of a square solar sail using two-DOF tip vane actuators have been studied in this paper. With control tip vanes, the solar sail's attitude and vibrations would remain controllable regardless of spacecraft's orientation with respect to the sunlight. One attitude controller and two attitude and vibrations controllers, based on collocated actuators and sensors, were presented for an undamped 150 m square solar sail with two-DOF control tip vanes.

Neglecting the actuators (tip vanes) dynamics, it was shown that (fast-responding or fast-rotating) control tip vanes could be useful for simultaneous attitude and vibrations controls. It is worth mentioning that it is possible that under some circumstances the dynamic moments due to rotation of the vanes could add up and become comparable with

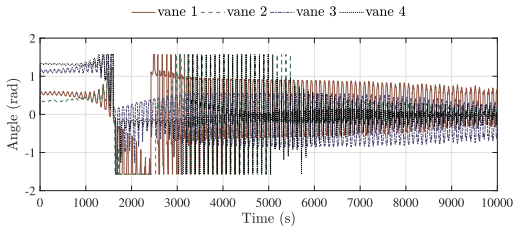

(a) First angular DOF of control vanes (α_1)

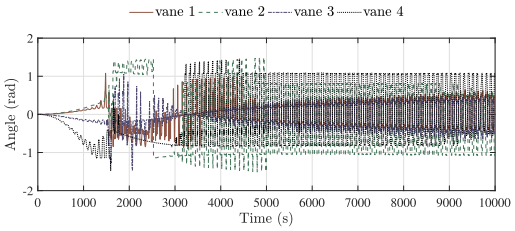

(b) Second angular DOF of control vanes (α_2)

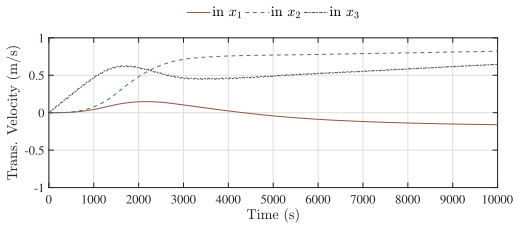

(c) Translational velocities at the center

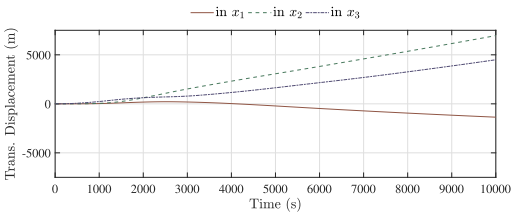

(d) Translational displacements at the center

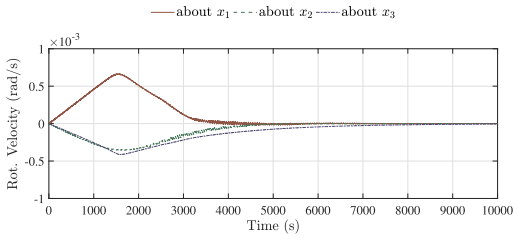

(e) Rotational velocities at the center

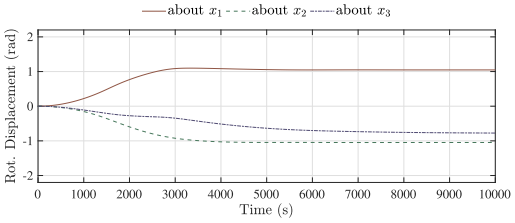

(f) Rotational displacements (Euler angles) at the center

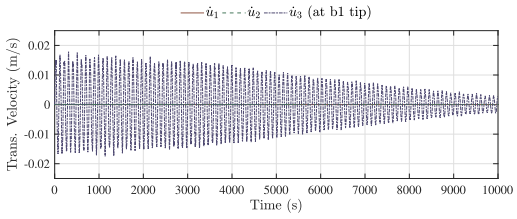

(g) Translational velocities at the tip of boom 1 (b1)

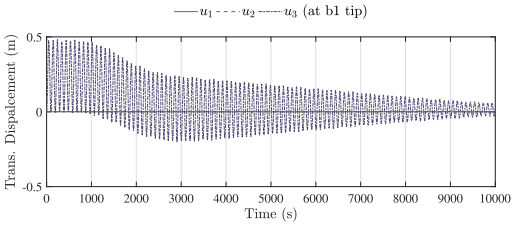

(h) Translational displacements at the tip of boom 1 (b1)

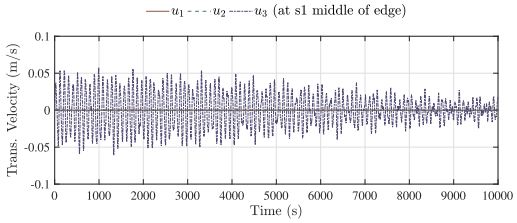

(i) Trans. velocities at the middle edge of sail 1 (s1)

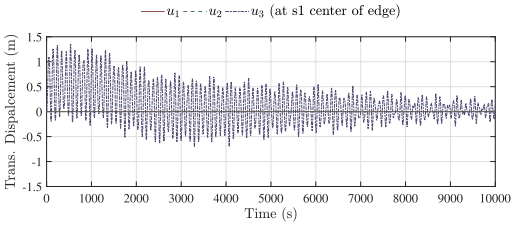

(j) Trans. displacements at the middle edge of sail 1 (s1)

Fig. 6. Solar sail dynamics with the second collocated attitude and vibrations controller (represented in $\mathcal{F}_B$) during the attitude maneuver from $\theta_1 = \theta_2 = \theta_3 = 0$ to $\theta_1 = \frac{\pi}{3}$, $\theta_2 = -\frac{\pi}{3}$, $\theta_3 = -\frac{\pi}{4}$.

the desired control efforts. However, examining such situations is beyond the scope of this paper and could be the subject of a future work.

Employing a finite-element-based linear structural model of the solar sail, the controller-structure interactions were examined. It was shown that none of the three developed controllers may destabilize the structural dynamics of the solar sail (due to control and observation spillover).

It was shown that a simple attitude and vibrations controller may add negative damping effects to the trajectory dynamics of a solar sail. Although no destabilization was observed in the presented numerical example, such negative damping effects may become important in the presence of a trajectory controller. An important conclusion drawn from this is the fact that developing and examining attitude and vibrations controllers for a flexible spacecraft based on pinned structural dynamic models (where the spacecraft's trajectory dynamics is neglected) may result in some difficulties and should be performed more carefully. It is worth mentioning that this is a common practice when developing attitude controllers for rigid spacecraft.

Finally, developing more advanced model-based optimal attitude and vibrations controllers and examining (combining) such controllers in the presence of (with) trajectory controllers are left to a future work.

Acknowledgments

This work was supported by the Natural Science and Engineering Research Council of Canada (NSERC).

Nomenclature

English Letters

F	Torque to force conversion (matrix)
R	Translational to rotational coordinates conversion (matrix)
T	Torque
U	Body frame displacement (position) with respect to inertial frame
V	Body frame velocity with respect to inertial frame
f	Force
J	Rotational inertia
k	Controller coefficient
m	Translational inertia (mass)
p	Position with respect to inertial frame
q	Generalized coordinate
s	Sun unit vector
t	Time
u	Elastic displacement with respect to body frame
w	Weighting coefficient
x	Spatial coordinate
y	Sensor measurements vector
z	Actuator actions vector

Calligraphic Letters

$\mathscr{B}$	Control input (matrix)
$\mathscr{C}$	Measurement output (matrix)
$\mathscr{F}$	Frame
$\mathscr{K}$	Stiffness (matrix)
$\mathscr{M}$	Mass (matrix)
$\mathscr{Q}$	Generalized force
$\mathscr{S}$	Unconstrained mode shapes (matrix)
$\mathscr{T}$	Generalized coordinates ransformation (matrix)

Greek Letters

Θ	Body frame rotational displacement with respect to inertial frame
Ω	Body frame rotational velocity with respect to inertial frame
α	Vane rotation (angular degree of freedom)
ε	Vector part of quaternion
η	Scalar part of quaternion
θ	Body frame Euler angle with respect to inertial frame
ω	Natural frequency

Leading/Post Subscripts/Superscripts

B	Body
I	Inertial
b	Boom
c	Control
d	Desired
e	Error
v	Vane

Others

$\boldsymbol{1}$	Identity (matrix)
$\square^{\times}$	Skew-symmetric matrix associated with a vector cross product
$\square^{T}$	Transpose operator

References

[1] M. Choi, C. Damaren, Structural dynamics and attitude control of a solar sail using tip vanes, J. Spacecr. Rocket. 52 (6) (2015) 1665–1679, https://doi.org/10.2514/1.A33179.
[2] B. Wie, D. Murphy, M. Paluszek, S. Thomas, Robust attitude control systems design for solar sails, part 2: MicroPPT-based secondary ACS, AIAA Guidance, Navigation, and Control Conference and Exhibit, Providence, RI, USA, 2004, https://doi.org/10.2514/6.2004-5011.
[3] B. Wie, D. Murphy, M. Paluszek, S. Thomas, Robust attitude control systems design for solar sails, part 1: propellantless primary ACS, AIAA Guidance, Navigation, and Control Conference and Exhibit, Providence, RI, USA, 2004, https://doi.org/10.2514/6.2004-5010.
[4] B. Wie, Solar sail attitude control and dynamics, part 1, J. Guid. Control Dyn. 27 (4) (2004) 526–535, https://doi.org/10.2514/1.11134.
[5] B. Wie, Solar sail attitude control and dynamics, part 2, J. Guid. Control Dyn. 27 (4) (2004) 536–544, https://doi.org/10.2514/1.11133.
[6] B. Fu, E. Sperber, F. Eke, Solar sail technology—a state of the art review, Prog. Aerosp. Sci. 86 (2016) 1–19, https://doi.org/10.1016/j.paerosci.2016.07.001.
[7] J. Baculi, M. Ayoubi, Fuzzy attitude control of solar sail via linear matrix inequalities, Acta Astronaut. 138 (2017) 233–241, https://doi.org/10.1016/j.actaastro.2017.05.021.
[8] N. Barnes, W. Derbes, C. Player, B. Diedrich, Sunjammer: a Solar Sail Demonstration, Springer, Berlin, Heidelberg, Germany, 2014, pp. 115–126, https://doi.org/10.1007/978-3-642-34907-2'8.
[9] M. Choi, C. Damaren, Control allocation of solar sail tip vanes with two degrees of freedom, J. Guid. Control Dyn. 39 (8) (2016) 1857–1865, https://doi.org/10.2514/1.G001703.
[10] Z. Kun, Control capability and allocation of solar sail tip vanes over bounded movement, J. Guid. Control Dyn. 38 (7) (2015) 1340–1344, https://doi.org/10.2514/1.G000938.
[11] O. Eldad, E. Lightsey, C. Claudel, Minimum-time attitude control of deformable solar sails with model uncertainty, J. Spacecr. Rocket. 54 (4) (2017) 863–870, https://doi.org/10.2514/1.A33713.
[12] S. Hassanpour, C. Damaren, Linear structural dynamics and tip-vane attitude control for square solar sails, J. Guid. Control Dyn. (2018) 1–15, https://doi.org/10.2514/1.G003485.
[13] D. Sleight, D. Muheim, Parametric studies of square solar sails using finite element analysis, 45th AIAA/ASME/ASCE/AHS/ASC Structures, Structural Dynamics & Materials Conference, Palm Springs, CA, USA, 2004, https://doi.org/10.2514/6.2004-1509.
[14] S. Thomas, M. Paluszek, B. Wie, D. Murphy, AOCS performance and stability validation for large flexible solar sail spacecraft, 41st AIAA/ASME/SAE/ASEE Joint Propulsion Conference & Exhibit, Tucson, Az, USA, 2005, https://doi.org/10.2514/6.2005-3926.
[15] Z. Jin, W. Tianshu, Coupled attitude-orbit control of flexible solar sail for displaced solar orbit, J. Spacecr. Rocket. 50 (3) (2013) 675–685, https://doi.org/10.2514/1.A32369.
[16] Z. Jin, Z. Kun, W. TianShu, Control of large angle maneuvers for the flexible solar sail, Sci. China Phys. Mech. Astron. 54 (4) (2011) 770–776, https://doi.org/10.1007/s11433-011-4277-1.
[17] S. Smith, H. Song, J. Baker, J. Black, D. Muheim, Flexible models for solar sail control, 46th AIAA/ASME/ASCE/AHS/ASC Structures, Structural Dynamics & Materials Conference, Austin, TX, USA, 2005, https://doi.org/10.2514/6.2005-1801.
[18] S. Hassanpour, C. Damaren, Linear structural dynamics and modal cost analysis for a solar sail, AIAA SciTech Forum, 5th AIAA Spacecraft Structures Conference, Kissimmee, FL, USA, 2018, https://doi.org/10.2514/6.2018-1434.
[19] R. Skelton, P. Hughes, Modal cost analysis for linear matrix-second-order systems, J.

Dyn. Syst. Meas. Control 102 (3) (1980) 151–158, https://doi.org/10.1115/1.3139625.
[20] P. Hughes, R. Skelton, Controllability and observability for flexible spacecraft, J. Guid. Control Dyn. 3 (5) (1980) 452–459, https://doi.org/10.2514/3.56020.
[21] P. Hughes, R. Skelton, Modal truncation for flexible spacecraft, J. Guid. Control Dyn. 4 (3) (1981) 291–297, https://doi.org/10.2514/3.56081.
[22] R. Skelton, P. Hughes, H. Hablani, Order reduction for models of space structures using modal cost analysis, J. Guid. Control Dyn. 5 (4) (1982) 351–357, https://doi.org/10.2514/3.19773.
[23] R. Garwin, Solar sailing—a practical method of propulsion within the solar system, Jet Propuls. 28 (3) (1958) 188–190 https://fas.org/rlg/030058-SS.pdf.
[24] C. McInnes, Solar Sailing: Technology, Dynamics, and Mission Applications, Springer-Verlag, New York, NY, USA, 1999, https://doi.org/10.1007/978-1-4471-3992-8.
[25] G. Greschik, M. Mikulas, Design study of a square solar sail architecture, J. Spacecr. Rocket. 39 (5) (2002) 653–661, https://doi.org/10.2514/2.3886.
[26] M. Balas, Feedback control of flexible systems, IEEE Trans. Autom. Control 23 (4) (1978) 673–679, https://doi.org/10.1109/TAC.1978.1101798.
[27] M. Balas, Trends in large space structure control theory: fondest hopes, wildest dreams, IEEE Trans. Autom. Control 27 (3) (1982) 522–535, https://doi.org/10.1109/TAC.1982.1102953.
[28] P. Hughes, Modal identities for elastic bodies, with application to vehicle dynamics and control, J. Appl. Mech. 47 (1) (1980) 177–184, https://doi.org/10.1115/1.3153599.
[29] G. Greschik, A linear photonic thrust model and its application to the L'Garde solar sail surface, 54th AIAA/ASME/ASCE/AHS/ASC Structures, Structural Dynamics & Materials Conference, Boston, MA, USA, 2013, https://doi.org/10.2514/6.2013-1803.
[30] B. Birge, Psot - a particle swarm optimization toolbox for use with matlab, Swarm Intelligence Symposium, Proceedings of the IEEE, IEEE, Indianapolis, IN, USA, 2003, pp. 182–186, , https://doi.org/10.1109/SIS.2003.1202265.